SUPPORTING INFORMATION

Dual NIR-I Excitation and Emission-Based Thermometry and pH-Responsive Drug Delivery Using $NaYF_4$:Yb,Er@SiO_2-Folic Acid Conjugates

*Sonali Mohanty[a,b], Ian Pompermayer Machado[a], Jorge García-Balduz[c], Simona Premcheska[a,c], Andre Skirtach[c], Kristof Van Hecke[b], Anna M. Kaczmarek[a]**

[a] NanoSensing Group, Department of Chemistry, Ghent University, Krijgslaan 281-S3, 9000 Ghent, Belgium

[b] XStruct, Department of Chemistry, Ghent University, Krijgslaan 281-S3, 9000 Ghent, Belgium

[c] NanoBioTechnology Group, Department of Biotechnology, Faculty of Bioscience Engineering, Ghent University, 9000 Ghent, Belgium

E-mail: Anna.Kaczmarek@UGent.be

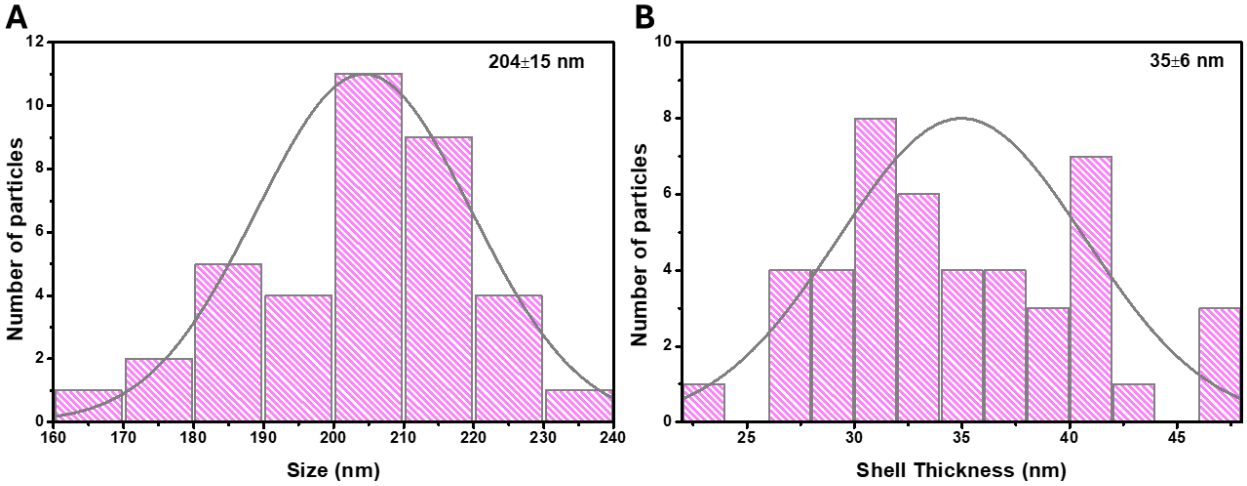

Figure S1. (A) Particle size distribution histograms for $NaYF_4$:Yb,Er and (B) SiO_2 shell thickness histogram for $NaYF_4$:Yb,Er@SiO_2.

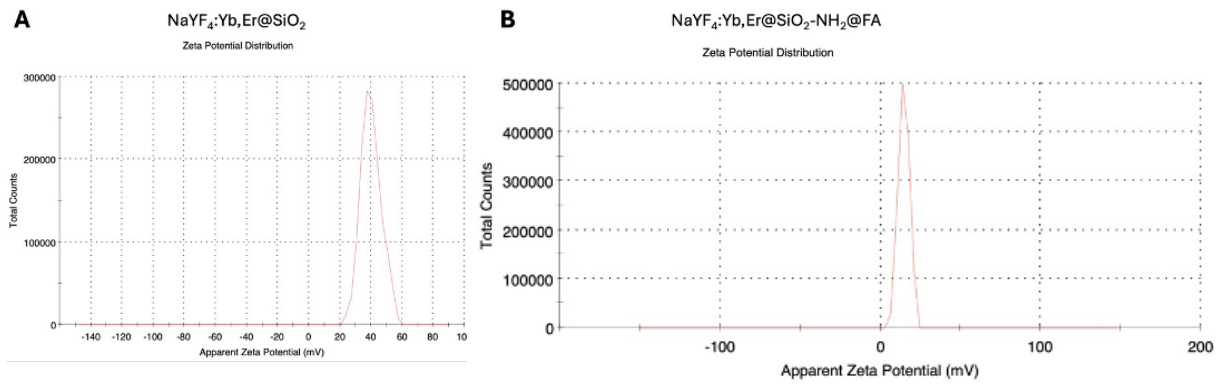

Figure S2. Zeta potential measurements of (A) $NaYF_4$:Yb,Er@SiO_2 and (B) $NaYF_4$:Yb,Er@SiO_2-NH_2@FA, showing surface charge changes after functionalization.

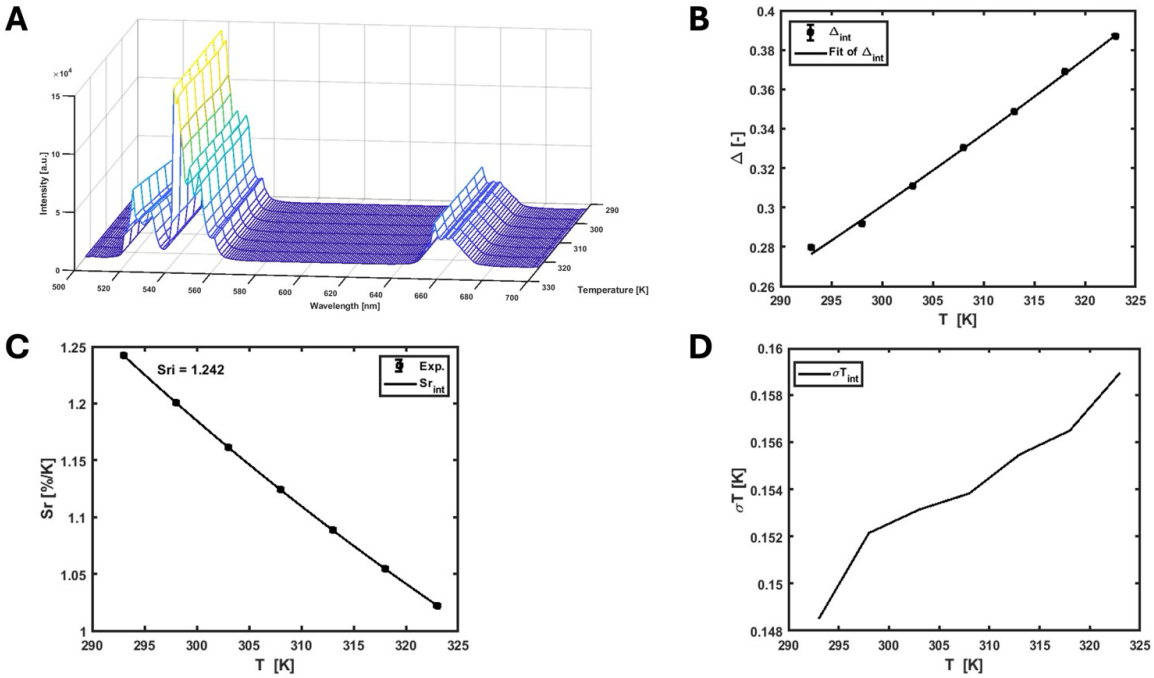

Figure S3. (A) Emission map of $NaYF_4$:Yb,Er dispersed in cyclohexane, recorded across the temperature range of 293.15–323.15 K (20–50 °C) in the visible region under 975 nm excitation, (B) graph showing the Δ parameter versus temperature. The points show the experimental Δ values, and the solid line shows the least squares fit to the experimental points. (C) Plot of the relative sensitivity (S_r) at varying temperatures. (D) Plot of the temperature uncertainty (σT) at varying temperatures.

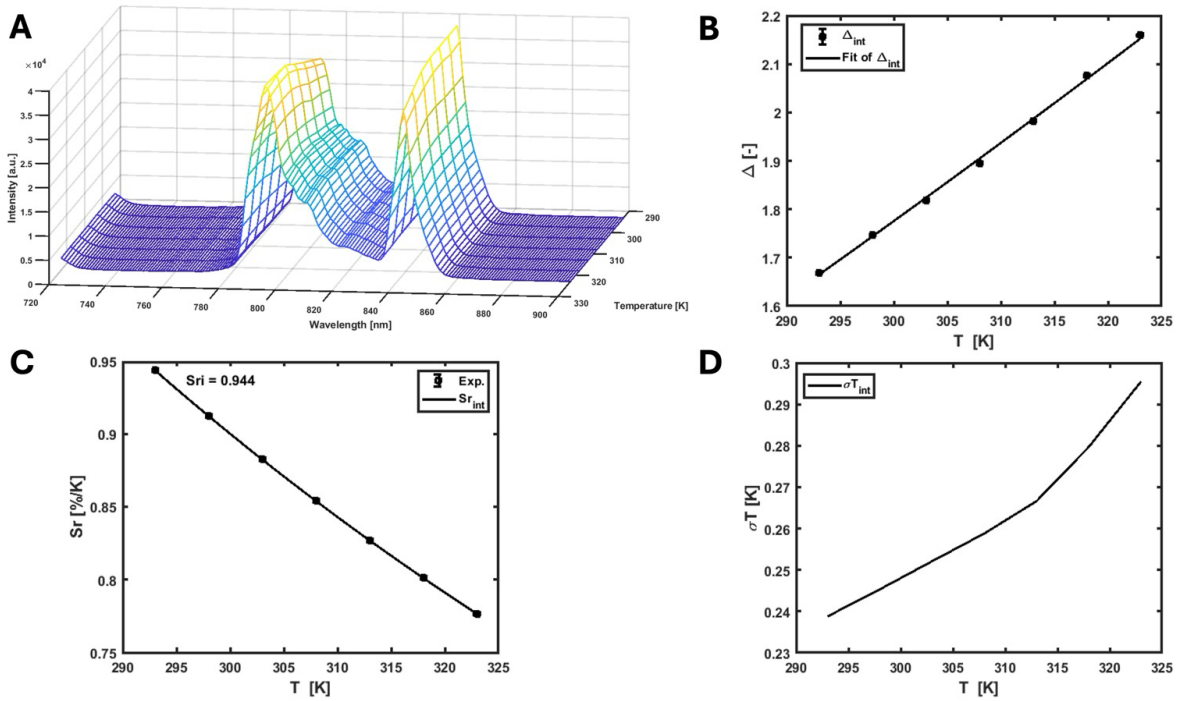

Figure S4. (A) Emission map of $NaYF_4$:Yb,Er dispersed in cyclohexane, recorded across the temperature range of 293.15–323.15 K (20–50 °C) in the NIR-I region under 975 nm excitation, (B) graph showing the Δ parameter versus temperature. The points show the experimental Δ values, and the solid line shows the least squares fit to the experimental points. (C) Plot of the relative sensitivity (S_r) at varying temperatures. (D) Plot of the temperature uncertainty (σT) at varying temperatures.

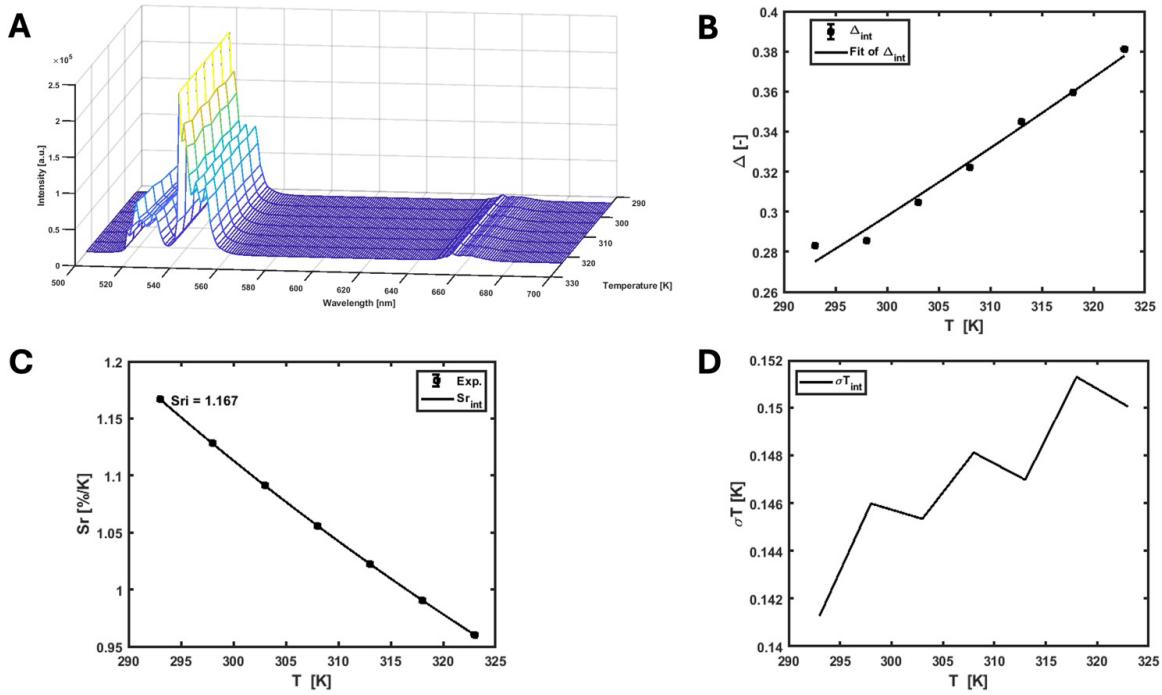

Figure S5. (A) Emission map of $NaYF_4$:Yb,Er dispersed in cyclohexane, recorded across the temperature range of 293.15–323.15 K (20–50 °C) in the visible region under 940 nm excitation, (B) graph showing the Δ parameter versus temperature. The points show the experimental Δ values, and the solid line shows the least squares fit to the experimental points. (C) Plot of the relative sensitivity (S_r) at varying temperatures. (D) Plot of the temperature uncertainty (σT) at varying temperatures.

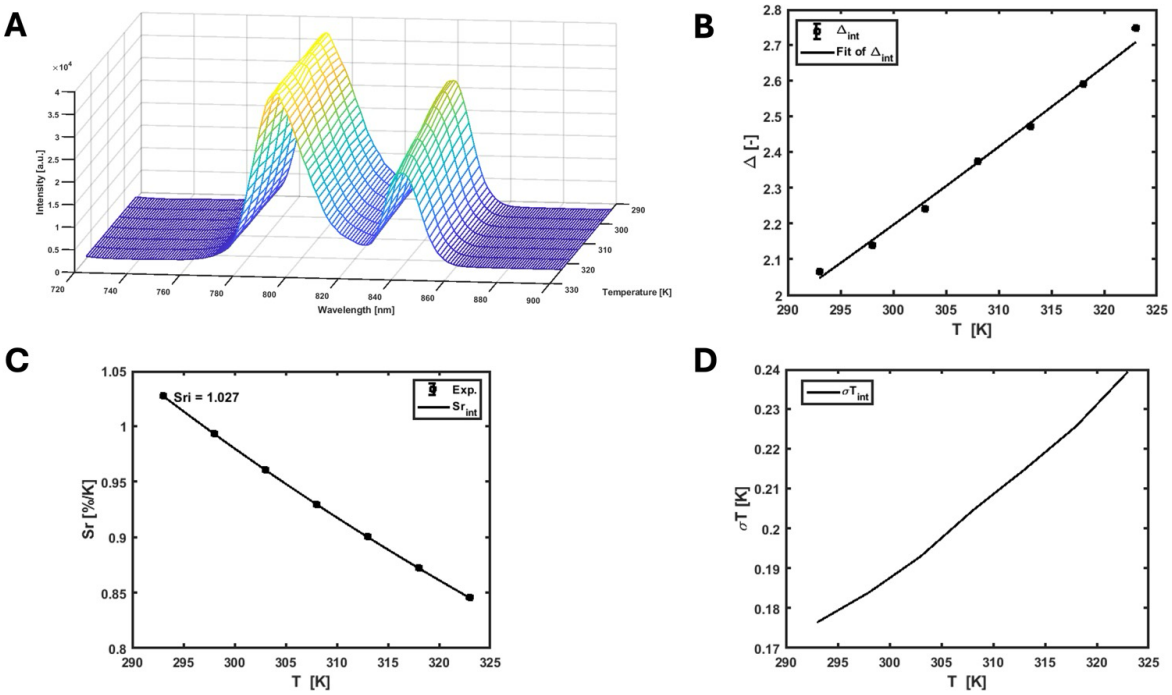

Figure S6. (A) Emission map of $NaYF_4$:Yb,Er dispersed in cyclohexane, recorded across the temperature range of 293.15–323.15 K (20–50 °C) in the NIR-I region under 940 nm excitation, (B) graph showing the Δ parameters versus temperature. graph showing the Δ parameter versus temperature. The points show the experimental Δ values, and the solid line shows the least squares fit to the experimental points. (C) Plot of the relative sensitivity (S_r) at varying temperatures. (D) Plot of the temperature uncertainty (σT) at varying temperatures.

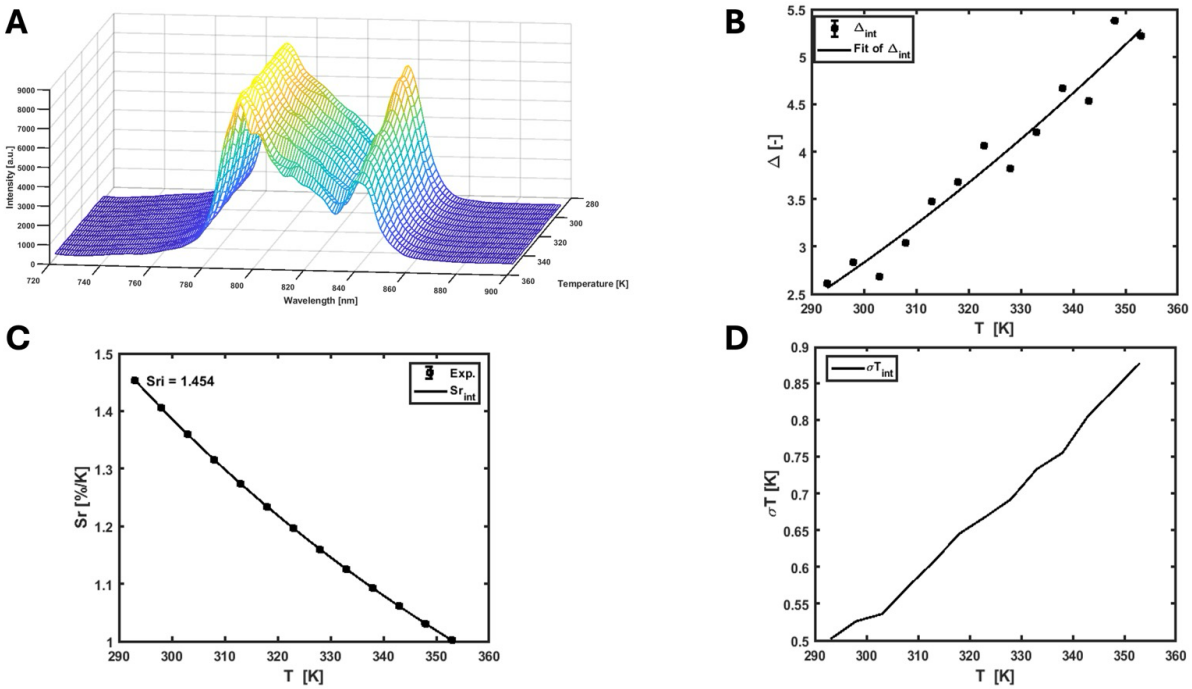

Figure S7. (A) Emission map of $NaYF_4$:Yb,Er@SiO_2 dispersed in water, recorded across the temperature range of 293.15–353.15 K (20–80 °C) in the NIR-I region under 940 nm excitation, (B) graph showing the Δ parameter versus temperature. The points show the experimental Δ values, and the solid line shows the least squares fit to the experimental points. (C) Plot of the relative sensitivity (S_r) at varying temperatures. (D) Plot of the temperature uncertainty (σT) at varying temperatures.

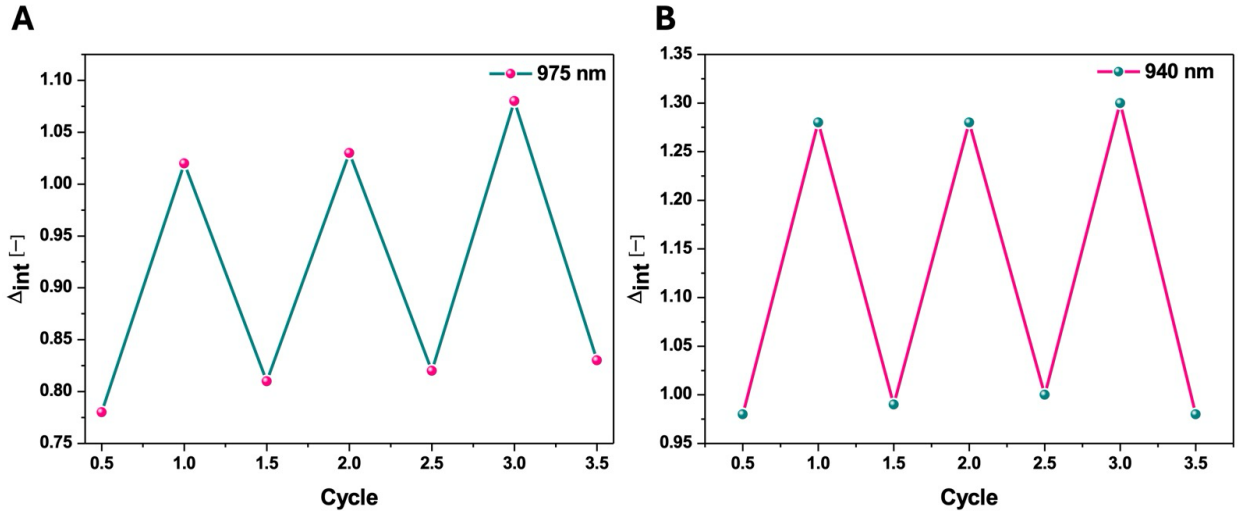

Figure S8. Cycle test for $NaYF_4$:Yb,Er@SiO_2-NH_2@FA in DI water under two heating–cooling cycles: 293.15 K–323.15 K, using excitation wavelengths of 975 nm and 940 nm.

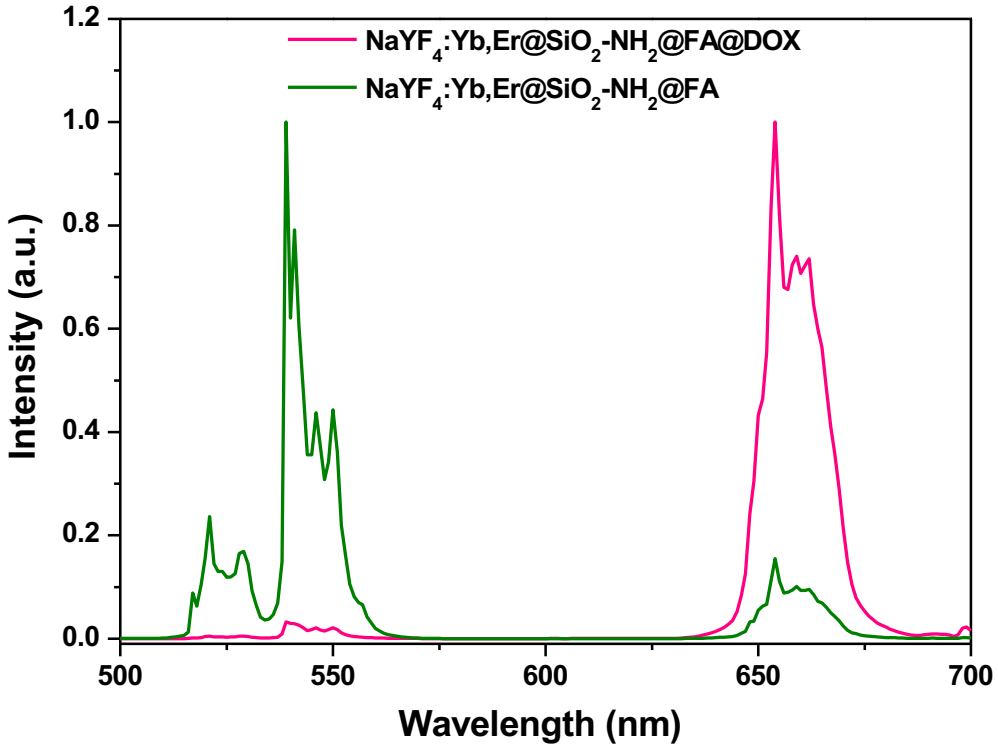

Figure S9. Upconversion emission spectra of $NaYF_4$:Yb,Er@SiO_2-NH_2@FA@DOX after DOX loading under 975 nm excitation. A clear drop in green emission is observed in the DOX loaded material, due to overall with DOX absorption in that region. This confirms close proximity of the DOX molecules to the Er^{3+} ions.

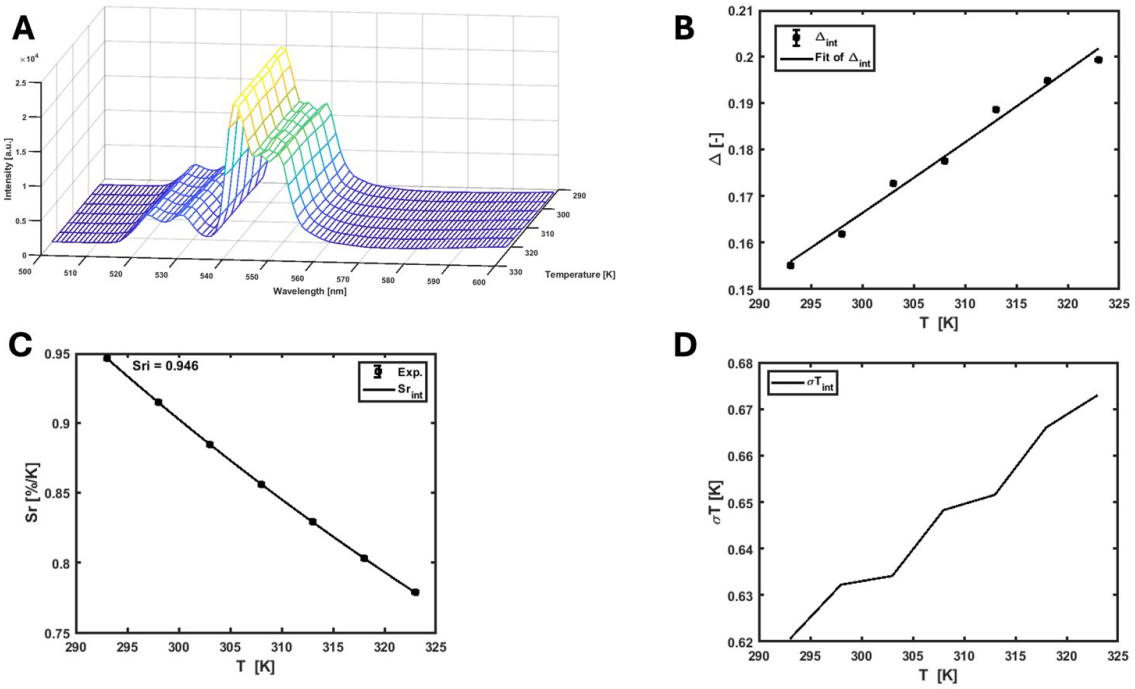

Figure S10. (A) Emission map of $NaYF_4$:Yb,Er@SiO_2-NH_2@FA@DOX dispersed in water, recorded across the temperature range of 293.15–323.15 K (20–50 °C) in the visible region under 975 nm excitation, (B) graph showing the Δ parameters versus temperature. graph showing the Δ parameter versus temperature. The points show the experimental Δ values, and the solid line shows the least squares fit to the experimental points. (C) Plot of the relative sensitivity (S_r) at varying temperatures. (D) Plot of the temperature uncertainty (σT) at varying temperatures.

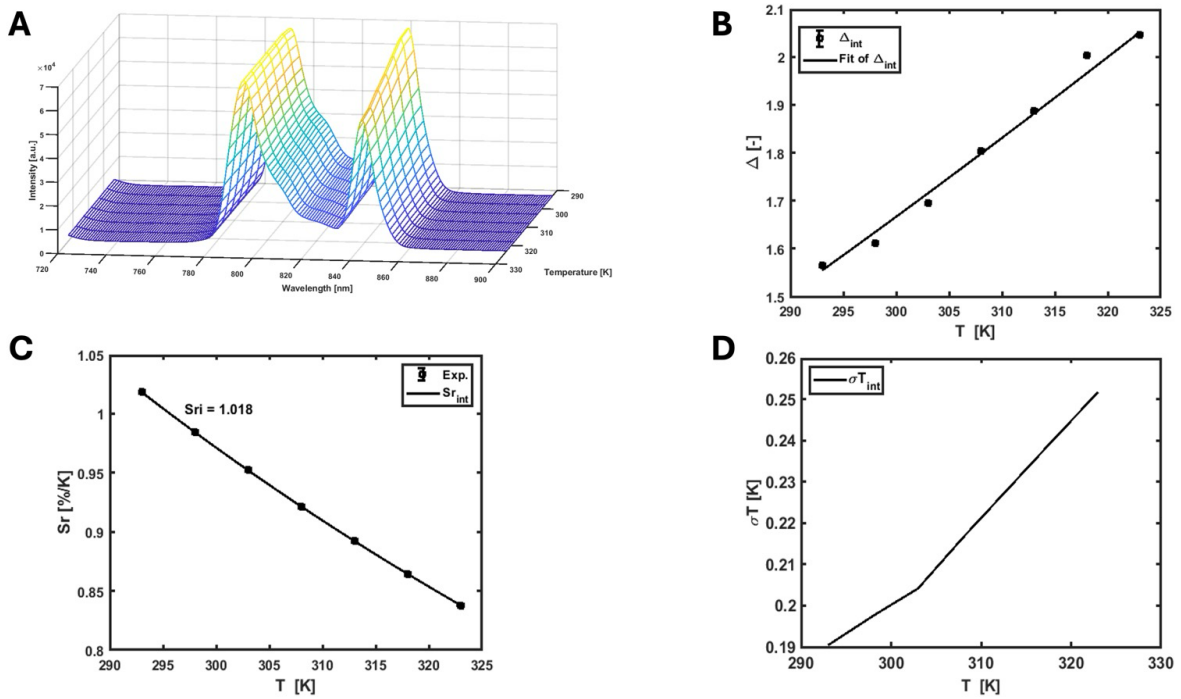

Figure S11. (A) Emission map of $NaYF_4$:Yb,Er@SiO_2-NH_2@FA@DOX dispersed in water, recorded across the temperature range of 293.15–323.15 K (20–50 °C) in the NIR-I region under 975 nm excitation, (B) graph showing the Δ parameters versus temperature. graph showing the Δ parameter versus temperature. The points show the experimental Δ values, and the solid line shows the least squares fit to the experimental points. (C) Plot of the relative sensitivity (S_r) at varying temperatures. (D) Plot of the temperature uncertainty (σT) at varying temperatures.

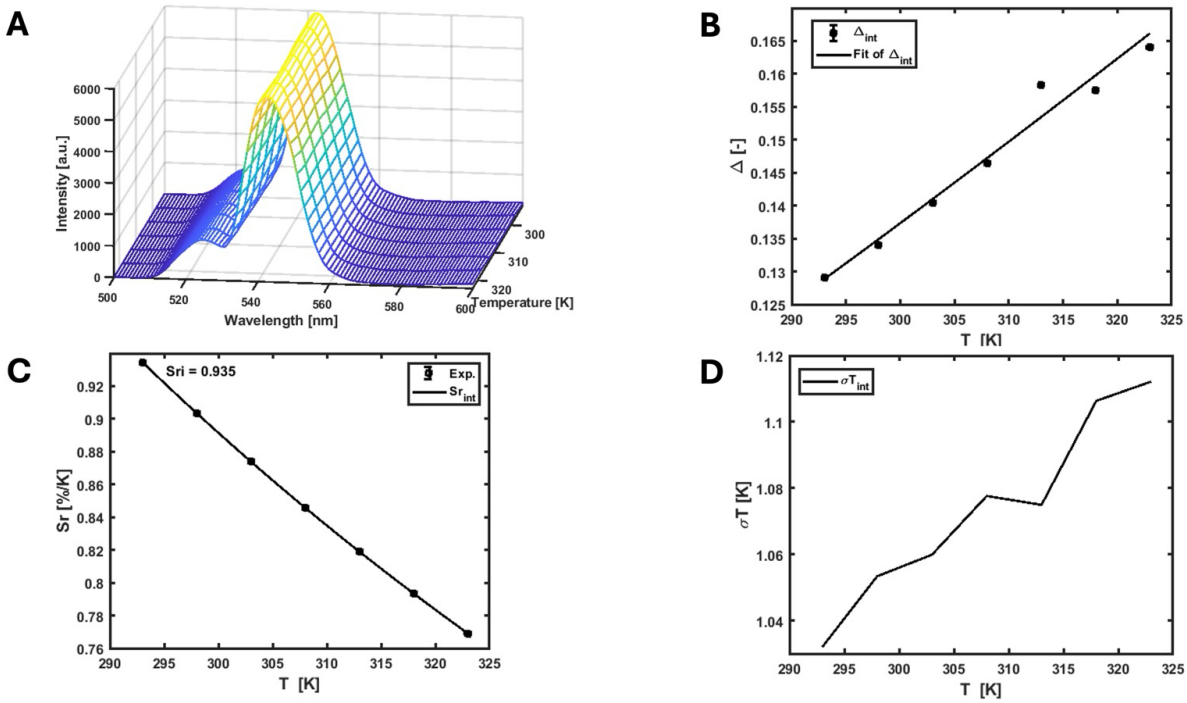

Figure S12. (A) Emission map of $NaYF_4$:Yb,Er@SiO_2-NH_2@FA@DOX dispersed in water, recorded across the temperature range of 293.15–323.15 K (20–50 °C) in the visible region under 940 nm excitation, (B) graph showing the Δ parameters versus temperature. graph showing the Δ parameter versus temperature. The points show the experimental Δ values, and the solid line shows the least squares fit to the experimental points. (C) Plot of the relative sensitivity (S_r) at varying temperatures. (D) Plot of the temperature uncertainty (σT) at varying temperatures.

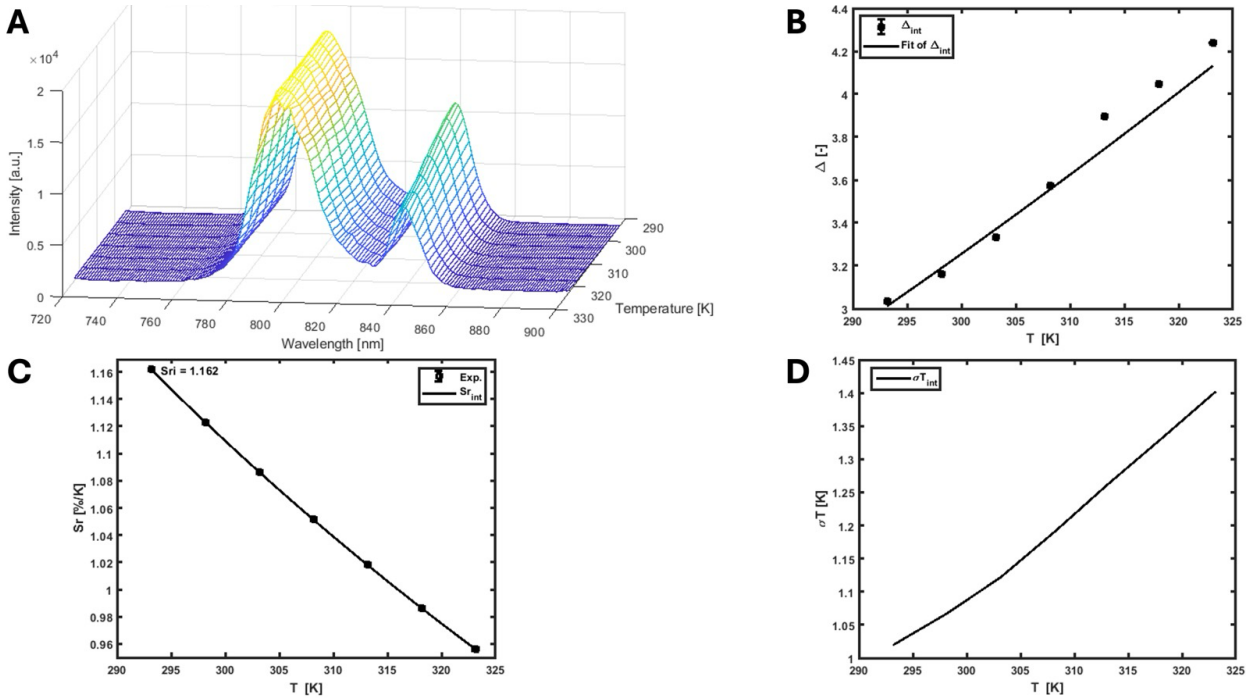

Figure S13. Emission map of $NaYF_4$:Yb,Er@SiO_2-NH_2@FA@DOX dispersed in water, recorded through chicken breast tissue (5 mm thickness at light entrance and exit) across the temperature range of 293.15–323.15 K (20–50 °C) in the NIR-I region ($^2H_{11/2}\rightarrow{}^4I_{13/2}$ and $^4S_{3/2}\rightarrow{}^4I_{13/2}$) under 975 nm excitation, (B) graph showing the Δ parameter versus temperature. The points show the experimental Δ values, and the solid line shows the least squares fit to the experimental points. (C) Plot of the relative sensitivity (S_r) at varying temperatures. (D) Plot of the temperature uncertainty (σT) at varying temperatures.

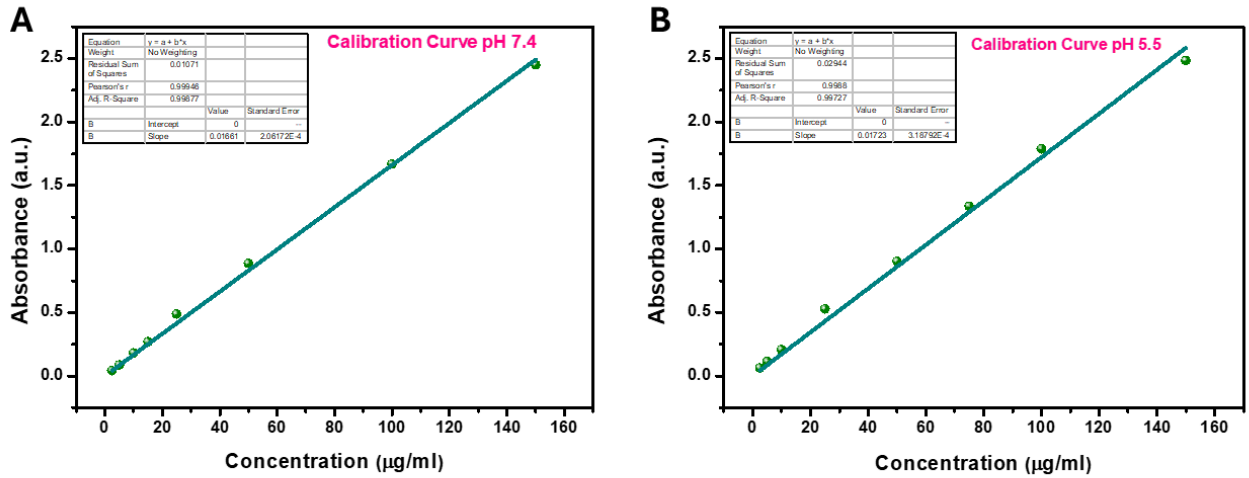

Figure S14. DOX calibration curves in PBS at (A) pH 7.4, and (B) pH 5.5.

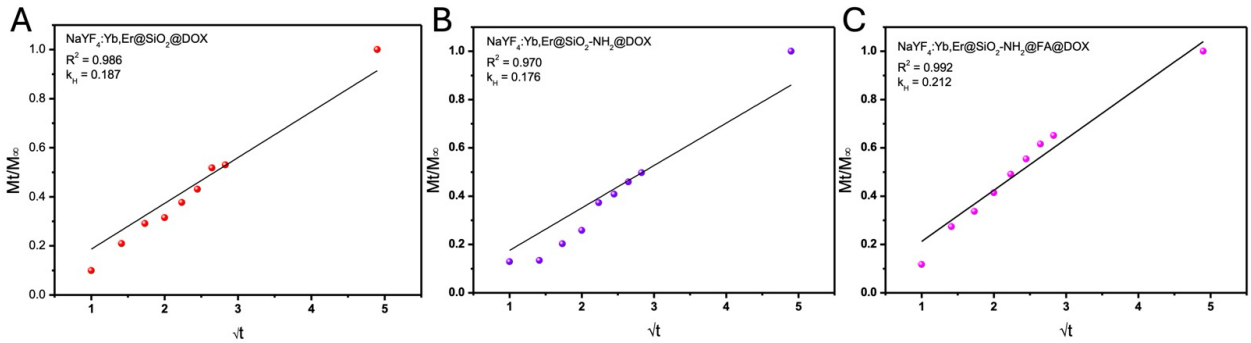

Figure S15. Higuchi kinetic model fitting of DOX release from (A) $NaYF_4$:Yb,Er@SiO_2, (B) $NaYF_4$:Yb,Er@SiO_2-NH_2, and (C) $NaYF_4$:Yb,Er@SiO_2-NH_2@FA particles at pH 5.5.

Table S1. Higuchi kinetic parameters (k_H, R^2) for DOX release from $NaYF_4$:Yb,Er@SiO_2, $NaYF_4$:Yb,Er@SiO_2-NH_2, and $NaYF_4$:Yb,Er@SiO_2-NH_2@FA particles at pH 5.5.

Sample	k_H	R^2
$NaYF_4$:Yb,Er@SiO_2@DOX	0.187	0.986
$NaYF_4$:Yb,Er@SiO_2-NH_2@DOX	0.176	0.970
$NaYF_4$:Yb,Er@SiO_2-NH_2@FA@DOX	0.212	0.992

Table S2. Korsmeyer–Peppas kinetic parameters (n, R^2) for DOX release from $NaYF_4$:Yb,Er@SiO_2, $NaYF_4$:Yb,Er@SiO_2-NH_2, and $NaYF_4$:Yb,Er@SiO_2-NH_2@FA particles at pH 5.5.

Sample	n (diffusional exponent)	R^2
$NaYF_4$:Yb,Er@SiO_2@DOX	0.78	0.978
$NaYF_4$:Yb,Er@SiO_2-NH_2@DOX	0.74	0.910
$NaYF_4$:Yb,Er@SiO_2-NH_2@FA@DOX	0.84	0.967

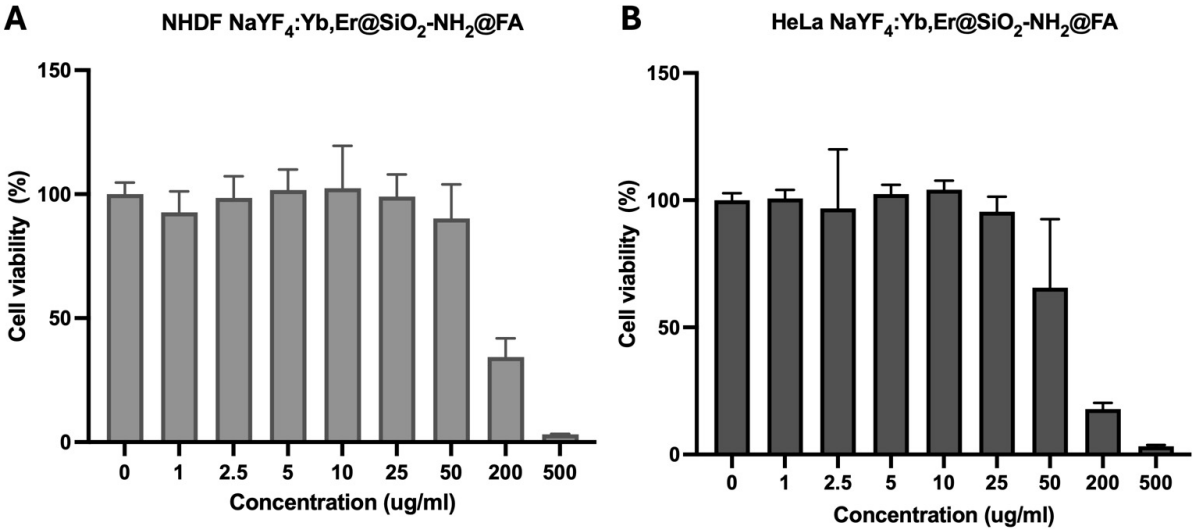

Figure S16. Cytotoxicity test results plotted as bar graph (mean + standard deviation) of the tested concentrations of $NaYF_4$:Yb,Er@SiO_2-NH_2@FA particles, ranging from 0-500 ug/mL on the chosen (A) NHDF and (B) HeLa cell line models. Statistical analysis applying the Mann-Whitney-Wilcoxon non-parametric test yielded no statistically significant differences between the medians of the control group and the median of every tested concentration group.